# Acoustic Study of a Sweeping Jet Actuator for Active Flow Control Applications

William C. Horne*, Nathan J. Burnside†
NASA Ames Research Center, Moffett Field, California, USA

## Abstract

**Active flow control for aircraft has been demonstrated to improve aerodynamic performance but generally introduces additional noise sources. This study presents measurements of the acoustic fields of sweeping jet actuators at full- and half-scale compared to the configuration recently demonstrated in ground- and flight-tests of a full-scale rudder. The effects of scale, flow rate, forward speed, and actuator synchronization state on tone and broadband noise directional power spectral density (PSD) levels are presented. The sweeping jet actuator PSD levels in the audio range increases as the second power of actuator flow rate. A fourth power variation of PSD level with flow rate is observed for a comparable non-sweeping actuator. These measurements will be used to develop noise source models for new aircraft configurations utilizing active flow control.**

## Nomenclature

$F_0$, $F_1$, $F_2$, .. - sweeping jet frequencies: fundamental and harmonics (first, second, ..)

M - free stream Mach number

$P_{AMB}$ - ambient pressure at actuator exit in pounds/inch$^2$ gauge (psig)

$P_{IN}$ – actuator inlet pressure in pounds/inch$^2$ gauge (psig)

PSD – power spectral density in dB/(Hertz$^{0.5}$) re 20x10$^{-6}$ Pa

R – microphone radius from source in inches

W – actuator volume flow rate in standard cubic feet per minute (SCFM)

$\theta$ – emission angle measured from upstream direction

$\phi$ – azimuth angle measured cross-stream from the direction normal to the actuator wall plate

## Background

Although various active flow control (AFC) configurations have demonstrated improved force and moment control for aircraft, they have yet to be utilized extensively on production aircraft due to added complexity, supply air requirements, and added noise. Recent improvements in capabilities of component and system level performance analysis and design tools are improving the prospects for including AFC in future aircraft, and it will become more important to understand and develop new tools for predicting and limiting AFC noise.

---

* Aerospace Engineer, Associate Fellow
† Aerospace Engineer, Senior Member

Sweeping jet fluidic oscillators have been recently considered for delaying flow separation on rudders [1, 2]. For a full-scale Boeing 757 rudder, 37 sweeping jet actuators were placed ahead of the rudder hinge line[1]. These

actuators had no moving parts, lower flow rates with comparable performance compared to steady flow actuators, and increased the maximum rudder control significantly compared to the non-actuated rudder. Since the rudder on a twin-engine aircraft is sized for control of the aircraft if an engine failed on take-off, this performance increase could allow a reduction in rudder area and associated weight for improved cruise performance. In this emergency scenario, actuator noise is a secondary concern.

Fig. 1a is a photograph of the rudder model installed in the Arnold Engineering Development Complex (AEDC) National Full-scale Aerodynamics Complex (NFAC) 40- by 80-Ft Wind Tunnel. During this test, the acoustic field in a horizontal plane intersecting the rudder at mid height was measured with six 24-element phased microphone arrays[3]. A typical hemispheric beamform map at 8 kHz is shown in Fig.
1b for the configuration with 6 actuators active, 100 kts. tunnel speed, 0˚ yaw and 0˚ rudder deflection.

Power spectral densities (PSDs) derived from 1/3-octave spectra and spatially integrated over the visible hemisphere from three of the arrays on the actuator side are presented in Fig. 2 (left). The positions of the three arrays relative to the rudder model are shown in Fig. 2(right). The PSDs from the three arrays show a strong fundamental and 1st harmonic at 250 and 500 Hz respectively, and broadband jet noise at higher frequencies. Arrays B2 and T2 (with windscreens) exhibit somewhat lower background noise levels at low frequencies than array K2 (no windscreen).

Sweeping jet AFC enhancement of high-lift systems has also been studied and performance improvements similar to those for the rudder have been demonstrated at small-scale[4, 5]. In this configuration, a smaller high-lift system with fewer elements using AFC can achieve similar high-lift performance as compared with conventional non-AFC designs that require larger multi-element flap systems. Wozidlo et al[3] present a detailed discussion of the basic actuator operation, including a high-resolution measurement of fundamental sweep frequency, $F_0$, vs. actuator flow rate that shows a piecewise-linear dependence for low flow rates (staging), and asymptotic approach to a constant saturation frequency at high flow rates.

There have been several recent studies of the detailed fluid mechanical behavior of the sweeping jet actuator. Wozidlo[3] and Koklu[6] investigated the effects of actuator and downstream surface geometry on such actuators for separation control. Kushner, et al[7] conducted a high-speed flow visualization study of a full-scale actuator used in the full-scale rudder test. The actuator exit measured 0.5 in. wide by 0.25 in. deep (1.27 x 0.635 cm), and was tested for pressure ratios $P_{IN}/P_{AMB}$ from 1.4 to 3.6. The visualization methods included particle image velocimetry (PIV) and laser speckle retroreflective background oriented schlieren (RBOS). The latter method generated time resolved images of the exit plume that compared well with an unsteady CFD simulation[7].

Despite many studies on the internal/external flow characteristics of the sweeping jet actuator and its effectiveness in improving the performance of aircraft rudder control and high-lift systems, there is a lack of understanding of the characteristics of the acoustic field needed to develop appropriate noise source models, aside from the full-scale rudder measurements previously mentioned. This report will present results of acoustic field measurements of sweeping- and non-sweeping jet actuators with effects of scale, flow rate, forward speed, and actuator synchronization. In addition to improved understanding of the noise sources for model development, the measurements can lead to strategies to mitigate AFC noise.

## Experimental Set-Up

Full- and half-scale actuators (relative to the full-scale rudder test and flow visualization study[7]) were mounted on a wall plate tangent to the inner surface of a 4 in. x 10 in. (10.16 x 25.4 cm.) nozzle exhausting into the Ames Experimental Aero-physics branch anechoic chamber, as shown in Fig. 3. The actuator exits were located 13 in. (33 cm.) downstream of the nozzle exit where the boundary layer thickness of the wall jet measured about 0.5" (1.27 cm). The full-scale actuator was built of nylon using stereo-lithography sintering (SLS). The half-scale actuators were machined from aluminum, as were the actuators in wind tunnel[1] and flow visualization experiments[7]. The anechoic chamber has Fiberglas wedges on all six sides, measures 25 ft. long x 18 ft. wide x 11 ft. high (7.62 x 5.49 x 3.35 m.), and is anechoic down to 250 Hz. The nozzle can deliver air to M = 0.19. The wall plate extended downstream 60 in. (1.52 m) and the wall trailing edge was serrated to minimize noise and flow instabilities associated with nozzle flow over the wall trailing edge
A variety of actuator configurations were tested, including:

- single full-scale sweeping jet actuator
- single half-scale sweeping jet actuator
- single half-scale non-sweeping jet actuator with same exit size as the sweeping jet
- dual half-scale sweeping jet actuators operating independently or synchronized in- and out-of-phase.

The half-scale non-sweeping jet actuator was tested to provide comparative acoustic measurements with a stationary jet source with the same exit geometry and similar operating conditions as with the sweeping jet configuration. This configuration is acoustically related to the full-span steady circulation control wing (CCW) studied by Horne and Burnside[8].

The half-scale sweeping and non-sweeping actuator internal flow paths are shown in Fig. 4. The sweeping jet actuator had an internal converging nozzle 5% smaller than at the exit. Synchronization of dual actuators was accomplished by adding auxiliary feedback tubes that cross-connected the two actuators as shown in Fig. 5. The original feedback path length for the half-scale actuators was approximately 2 in. (5.08 cm), the added auxiliary tubes were each about 10.75 in. (27.3 cm) long and consisted of ¼" ID plastic tubing. The sweep frequency dropped by about 10% when the auxiliary tubes were added. The cross-connecting scheme is similar to (but simpler than) the design of Koklu[9] that used accumulators and additional connections not used in the present study. The objective in this study was to provide well-defined phase relationships between the two actuators during the measurements, particularly for tones. It should be noted that measured tone levels were quite sensitive to flow rate and installation details as compared to the broadband levels.

A flow system capable of providing 100 standard cubic ft./min. (SCFM) or 2.83 std. $m^3$/min. at 100 psig (689.4 kPa) was connected to actuator inlets through the nozzle wall. Flow rates in were measured with Hedland direct reading flow meters and corrected for variations in supply pressure and temperature to 2% of full scale. The flow meters were calibrated independently with a precision hot-wire calibration nozzle and also used to calibrate the actuator pressure drop as an alternate flow rate measurement. The flow was controlled with Wilkerson electronic flow regulators as also used on the full-scale rudder test[1] and the flow visualization study[7].

The acoustic field was measured with a fixed array of G.R.A.S. 40BF ¼" diameter free field microphones with G.R.A.S. 26AC preamplifiers. The microphones were placed at radii R of 96 and 48 in. (2.44 and 1.22 m.) at emission angles θ of 67.5˚, 90˚, 112.5˚, 135˚. 157.5˚, and azimuth angles, ϕ (at R = 48", θ = 90˚) of 0˚, +/- 22.5˚, +/- 45˚, and +/- 90˚. The microphones were positioned at the same elevation at each emission angle. Some full-scale actuator measurements were acquired at r = 96", most full-scale and all half-scale actuator measurements were taken at r = 48". Data was acquired at 100 kHz bandwidth with a National Instruments 24-bit synchronous A/D system. Electret microphones were also imbedded in the wall plate at 33 locations and these signals were acquired at the same time as the field microphones. Analysis of the surface pressure signals is in progress and will be reported at a later date.

## Results

The fundamental oscillation frequency, $F_0$, of the actuators was measured with the far-field sensors and with surface pressure transducers position near the actuator exits. The frequency varied initially linearly with flow rate, then asymptotically approached a saturation limit, as shown in Fig. 6. This plot compares data from the full-scale actuator of the flow visualization study[7] (smooth aluminum), the full-scale actuator from the present acoustic study (rougher SLS surface), and data from the half-scale actuators scaled to full-scale by plotting the frequency/2 vs four times the flow rate of the half-scale actuators. All of the smooth aluminum actuators exhibited a similar frequency vs flow rate characteristic, with a full-scale saturation frequency of ~250 Hz similar to the measurement of the full-scale rudder in the wind tunnel. The SLS full-scale actuator reached a saturation frequency of 268 Hz (7.2% increase) for reasons not understood but possibly related to the rougher SLS surfaces of the internal flow channels. When scaled to full size, the half-scale aluminum actuator frequency characteristic was similar to the aluminum full-scale actuators of the full-scale wind tunnel test[1] and flow visualization study[7]. The frequency vs flow rate characteristic of Fig. 6 is similar to results of other studies of comparable geometries [4, 10]. Von Gosen et al[11] observed that the non-linear frequency-vs- flow rate curve is actually linear when frequency is plotted against exit Mach number, terminating at an exit Mach number of 1.

Fig. 7 presents PSDs of the full scale actuator with input of 25 psig, 73 SCFM, at an emission angle of 90˚ measured from broadside (left, $\phi = 0^{\circ}$) and sideline (right, $\phi = 90^{\circ}$). In the broadside direction, the fundamental was about 15 dB weaker than the 1st harmonic, and higher harmonics were absent. The strong 1st harmonic (twice the sweep frequency) could arise from a periodic modulation of the exit flow rate at this frequency, or a sweeping jet motion that was more similar to a square-wave than a sinusoid. In comparison, the fundamental level for the full-scale rudder (Fig. 2, left) was comparable to the 1st harmonic level, and higher harmonics were not visible. The rudder data included contributions from 6 actuators spaced along the rudder hinge line, with a range of $\theta$ and $\phi$.

In the sideline direction, the fundamental is about 13 dB louder than the 1st harmonic, and higher harmonics up to the 7th are visible above the broadband noise. The rich harmonic content in this direction is also consistent with non-sinusoidal jet motion. The broadband noise peaks at 7-8 kHz at about 60 dB and approximately 20 dB below the tone peaks. Also shown in Fig. 7 are the effects of simulated forward speed of M = 0.15 (blue curves) that results in 3-4 dB reduction of the broadband noise level relative to the case for M = 0 (red curves). A slight reduction in tone level but no apparent frequency shift is observed with forward speed.

1/12th octave directivities of the tone levels in selected planes are presented for the full- and half-scale single actuators in Fig 8 ($\theta = 90^{\circ}$) and Fig. 9 ($\phi = 0^{\circ}$). The full-scale flow rate was 40 SCFM, the highest flow rate for which the half- and full-scale sweep frequencies were scalable (Fig. 6). Between the full- and half-scale actuators, the fundamental (black), 1st harmonic (blue), and 2nd harmonic (red) tone levels exhibit overall similarities in the pattern shapes, but some differences in relative levels between the two scales. In the $\theta = 90^{\circ}$ plane, the fundamental and 2nd harmonic have the character of a vertical dipole. The 1st harmonic dominates the directivity in the $\phi = 0^{\circ}$ plane, since the fundamental and 2nd harmonic are minimum there. The 1st harmonic level in this plane increases towards the downstream direction.

Fig. 10 shows the directivities of the fundamental tone in the same planes for the single half-scale actuator (solid black) and dual half-scale actuators operating independently (dashed black), in-phase (red) and out-of-phase (blue) for 10 SCFM, the same scaled flow rate as Fig. 8 and 9. The auxiliary feedback ducts were in place for all three conditions. As expected, the tones from the two independent actuators are louder (but not by as much as 3 dB) in the $\theta = 0^{\circ}$ plane, and less clearly related in the $\theta = 0^{\circ}$ plane near the minimum level. When operated in phase, the fundamental is nearly cancelled in the broadside direction, $\theta = 90^{\circ}$, $\phi = 0^{\circ}$, but increases in other directions away from $f = 0^{\circ}$. Operating the jets out of phase achieves the same fundamental level as the independent jets in the broadside direction, and levels at directions away from $\phi = 0^{\circ}$ are reduced by 3-5 dB relative to the independent jets.

Variations in the 1st harmonic are less pronounced than for the fundamental and 2nd harmonics, as shown in Fig. 11. Fig. 11 shows some reduction in level for the dual independent actuators relative to the single actuator in both the $\theta = 90^{\circ}$ and $\phi = 0^{\circ}$ planes. Peak radiation is roughly at $\phi = 120^{\circ}$ emission angle in Figs. 10 and 11. It should be noted that more variability was noted for tone levels compared with broadband levels possibly due to tone dependence on parameters such as flow rate, typical of some resonant systems.

It was decided to compare the broadband noise of the sweeping jet with that of a non-sweeping jet issuing from an identically sized exit, as shown in Fig. 4. The same exit geometry was preserved so that the flow exiting the non-sweeping jet actuator encountered an abrupt +/- 45˚ lateral expansion that precluded the jet from remaining attached to the exit walls. The pressure drops (actuator inlet – ambient) through the sweeping and non-sweeping half-scale jets are presented in Fig. 12. Both actuators exhibited quadratic dependence of pressure drop vs. flow rate. With the available range in flow rate, the non-sweeping jet actuator saw a maximum pressure ratio (exit total/exit static) of 2.66 at a flow rate of 24.8 SCFM (0.702 std. $m^3$/min.), corresponding to a fully expanded Mach number of 1.27. Higher pressure losses for the same flow rates were observed for the sweeping jet actuator; from twice as much at low flow rates to about 75% higher at the highest flow rates. Also noted on Fig. 12 are 3 conditions for comparison of corresponding PSDs:

1. sweeping jet at 14 SCFM, $P_{IN} = 17.8$ psig
2. non-sweeping jet at the same flow rate as 1 (14 SCFM), $P_{IN} = 9.3$ psig
3. non-sweeping jet at a similar inlet pressure as 1 (17.5 psig), flow rate = 10.5 SCFM.

Power spectral densities of the broadside microphone ($\theta = 90^{\circ}$, $\phi = 0^{\circ}$) for these conditions are shown in Fig. 13. The loudest signal (tones and broadband) is for the sweeping jet (1). The broadband levels for the non-

sweeping jet have a similar shape, but are about 3 dB lower for the matched pressure condition (2), and about 10 dB lower for the matched flow rate condition (3). For the non-sweeping jet, choking is predicted for an exit pressure ratio $P_{IN}/P_{AMB} = 1.893$, or $P_{IN} = 13.1$ psig.

These measurements may also be used to derive simple scaling rules for PSD broadband level as a power of the flow rate, without frequency scaling. For the non-sweeping jet, Fig. 14 shows data from the microphone at $\theta = 90^\circ$, $\phi = 45^\circ$, for flow rates of 7.1, 15.9, 20.9, and 23.4 SCFM with as much as 25 dB difference between spectral levels from 0.1 to 20 kHz. Applying a 4th power scaling of flow rate ($+40 \log(W/W_{REF})$ collapsed the PSDs for all but the lowest flow rate, and that PSD collapsed with the others fairly well from 1 kHz to 4 kHz.

For the half-scale sweeping jet, the best collapse over from 0.1 to 5 kHz appears to be for 2nd power scaling with flow rate, as seen in Fig. 15 for the microphone at $\theta = 90^\circ$, $\phi = 45^\circ$. The flow rates for these data are 8.2, 12.1, and 19.4 scfm. A similar collapse is observed for the second power of flow rate at $\theta = 157.5^\circ$, $\phi = 45^\circ$, as shown in Fig. 16. Beyond the frequency ranges of simple 2nd or 4th power scaling collapse, the peak broadband frequencies shift higher with increasing flow rate, and the PSD levels also rise faster with flow rate after scaling.

For subsonic operation, the non-sweeping jet exit pressure and density should be approximately the same as ambient conditions, and the exit velocity is the flow rate divided by exit area. The total pressure loss through the non-sweeping actuator varied from 15% at low flow rates to a minimum of 8% at higher flow rates. After choking, the exit velocity is fixed, and further increases in supply pressure only increase the density of the underexpanded exit plume[11]. For the sweeping jet, the complex internal flow and higher pressure loss further complicates the picture. The simple power law scalings described above are intended only to provide engineering estimates of noise levels at low frequency range relevant to noise control, and not the basis of a physical noise model. In particular higher frequency measurements would be needed to confirm 8th power velocity scaling for the subsonic non-sweeping jet. In addition, the scaling is expected to differ for actuators directing air over a finite-length deflected control surface rather than the long, undeflected wall of the present study.

## Concluding Remarks

Acoustic surveys of the acoustic field of single- and dual-sweeping jet actuators were conducted in the NASA Ames Research Center anechoic chamber. The actuators were full- and half-scale size relative to those recently demonstrated on a full scale Boeing 757 rudder in recent wind-tunnel and flight tests, and associated flow visualization studies. The effects of simulated forward speed and independent and synchronized operation of the dual actuators was also studied. Simulated forward speed up to M = 0.19 resulted in a slight decrease in broadband noise levels. The tone fundamental frequency was found to vary with inlet pressure and flow rate in a manner similar to previous studies of actuators with similar geometry and construction, however rougher internal surfaces with 3D-printed actuators resulted in higher sweep frequency. Directivities of tones and broadband noise were measured with a fixed array of microphones. For the audio frequency range, the non-sweeping actuator broadband spectral levels scaled with flow rate to the 4th power, while sweeping-jet actuator broadband spectral levels best scaled with flow rate to the 2nd power. Flow rate scaling was less effective for tone levels than for the broadband levels.

## Acknowledgements

This research was funded by the NASA Advanced Air Transport Technology (AATT) High-Aspect Ratio Wing (HARW) program. The authors acknowledge the constructive guidance from other program participants including John C. Lin, Craig Hunter, and Taylor Spalt.

## References

1. “Performance Enhancement of a Full-Scale Vertical Tail Model Equipped with Active Flow Control”, Whalen, E., Lacy, D., Lin, J., Andino, M., Washburn, A., Graff, E., and Wygnanski, I., AIAA-2015-0784, AIAA SciTech – 53st Aerospace Sciences Mtg. , 5-9 Jan. 2015, Kissimmee, FL.

2. “Performance Enhancement of a Vertical Tail Model with Sweeping Jet Actuators”, Seele, R., Graff, E., Lin, J., Wygnanski, I., AIAA-2013-0411, 51st AIAA Aerospace Sciences Meeting, 7-10 Jan. 2013, Grapevine, TX.

3. **“**Innovative, Low-cost Phased Microphone Array Design for Moderate-Scale Aeroacoustics tests”, Horne, W., and Burnside, N., NASA Aeronautics Research Institute, Feb. 2014, http://nari.arc.nasa.gov/node/30

4. “On the Use of Sweeping Jets to Augment the Lift of a l-Wing”, Tewes, P., Taubert, L., and Wygnanski, I., AIAA-2010-4689, AIAA 28th Applied Aerodynamics Conf., 28 June – 1 July 2010, Chicago, IL.

5. “Parametric Study of Sweeping Jet Actuators for Separation Control”, Woszidlo, R., Nawroth, H., Raghu, S., AIAA-2010-4247, AIAA 5th Flow Control Conference, 28-June-1 July 2010, Chicago, IL.

6. “The effects of Sweeping Jet Actuator Parameters on Flow Separation Control”, Koklu, M., AIAA-2015-2485, AIAA Aviation – 45th Fluid Dynamics Conf., 23-26 2015, Dallas, TX.

7. “Visualization of a Sweeping Jet by Laser Speckle Retro-reflective Background Oriented Schlieren”, Kushner, L., Heineck, J., Storms, B., and Childs, R., AIAA-2015-1697, AIAA SciTech – 53rd Aerospace Sciences Mtg. , 5-9 Jan. 2015, Kissimmee, FL.

8. “AMELIA CESTOL Test: Acoustic Characteristics of Circulation Control Wing with Leading- and Trailing-Edge Slot Blowing”, Horne, W., and Burnside, N., AIAA-2013-0978, 51st AIAA Aerospace Sciences Mtg., 07-10 Jan. 2013, Grapevine, TX.

9. “Fluidic Oscillator Array for Synchronized Oscillating Jet Generation”, US Patent 20150238983 A1, 27 Aug., 2015

10. “Experimental Comparison between the Flow Field of Two Common Fluidic Oscillator Designs”, Osterman, F., Woszidlo, R., Nayeri, C., and Paschereit, C., AIAA-2015-0781, AIAA SciTech-53rd AIAAA Aerospace Sciences Mtg., 5-9 Jan. 2015, Kissimmee, FL.

11. “Experimental Investigation of Compressibility Effects in a Fluidic Oscillator”, von Gosen, F., Osterman, F., and Woszidlo, R., AIAA-2015-0782, AIAA SciTech-53rd AIAAA Aerospace Sciences Mtg., 5-9 Jan. 2015, Kissimmee, FL.

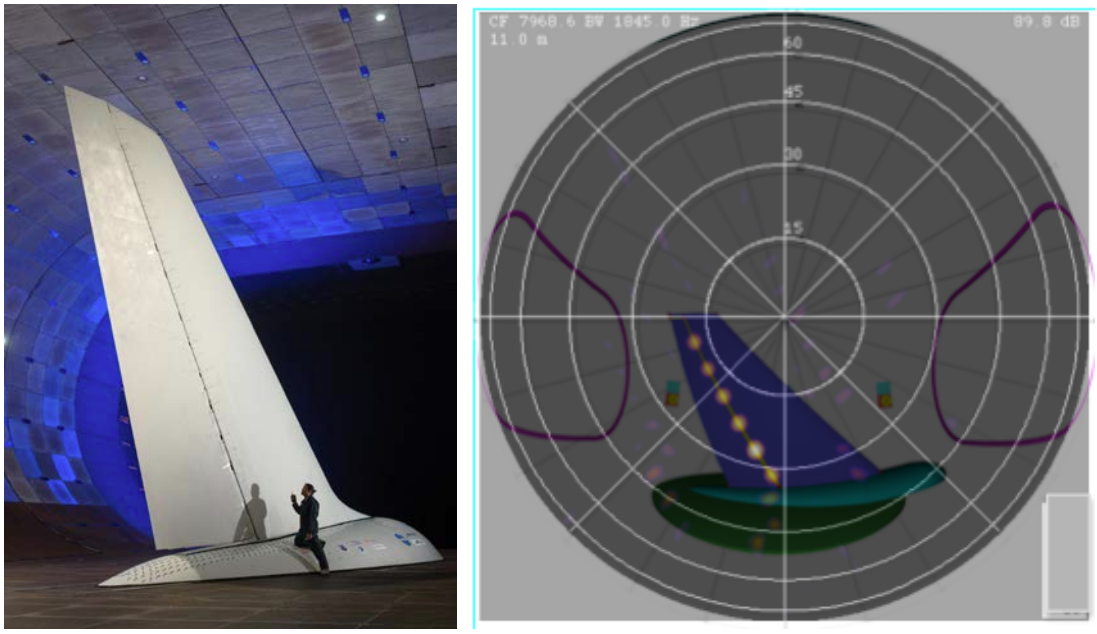

1a. 1b.

Fig. 1a. Full-scale rudder with 37 fluid actuators mounted upstream of rudder hinge line.
Fig. 1b. Hemispheric noise source location map for rudder with 6 active actuators at 100 kts, 0˚ yaw/deflection angle, 8 kHz.

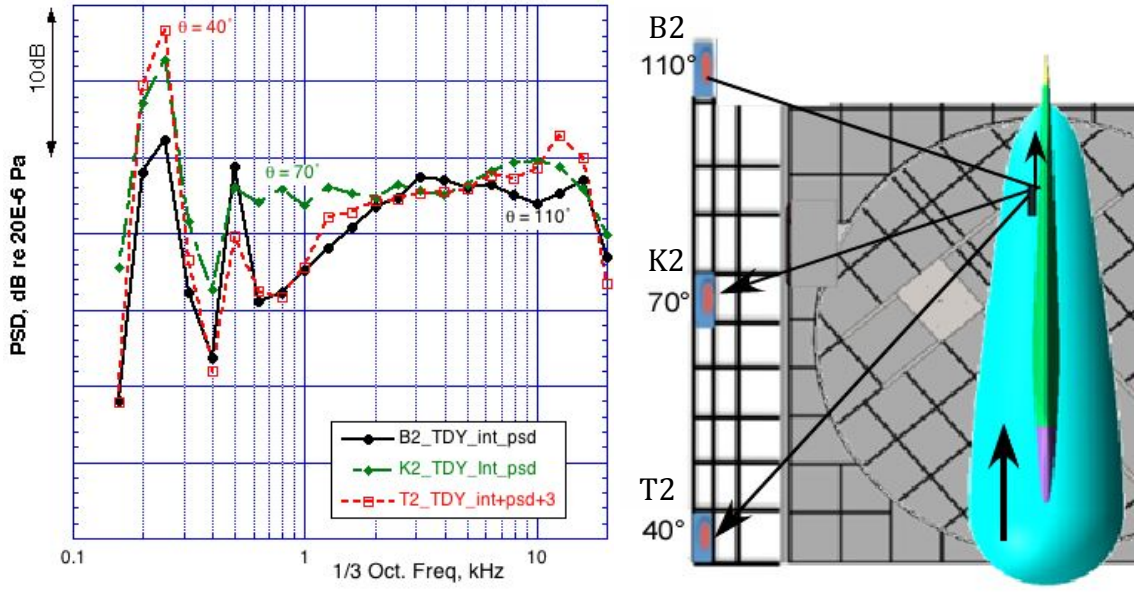


Fig. 2 Array spectra from the configuration of Fig. 1(6 active actuators), at emission angles of 110˚ (black), 70˚ (green), and 40˚ (red). The levels are scaled to the same distance.

3a. 3b.

Fig. 3. 4” x 10” jet nozzle with wall plate extensions:
3a – single full-scale actuator (overlay shows outline of internal flow channels)
3b – dual half-scale actuators, with internal flow outline overlays

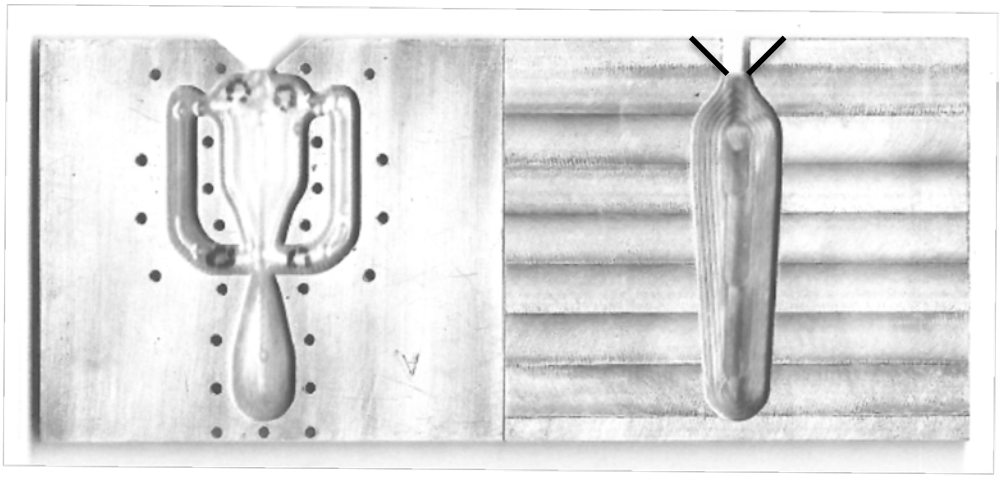

Fig. 4. Half-scale actuators: sweeping jet (left) and non-sweeping jet (right)

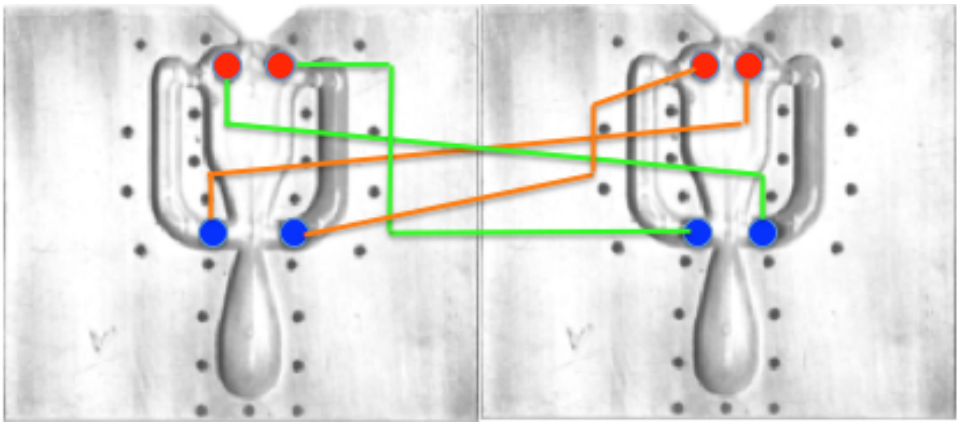

Fig. 5. Half-scale sweeping jet acutor, cross connected for synchronized out-of phase operation, bypass tubes connect downstream ports to opposite-side upstream ports. For synchronized in-phase operation, bypass tubes connect downstream ports to same-side upstream ports.

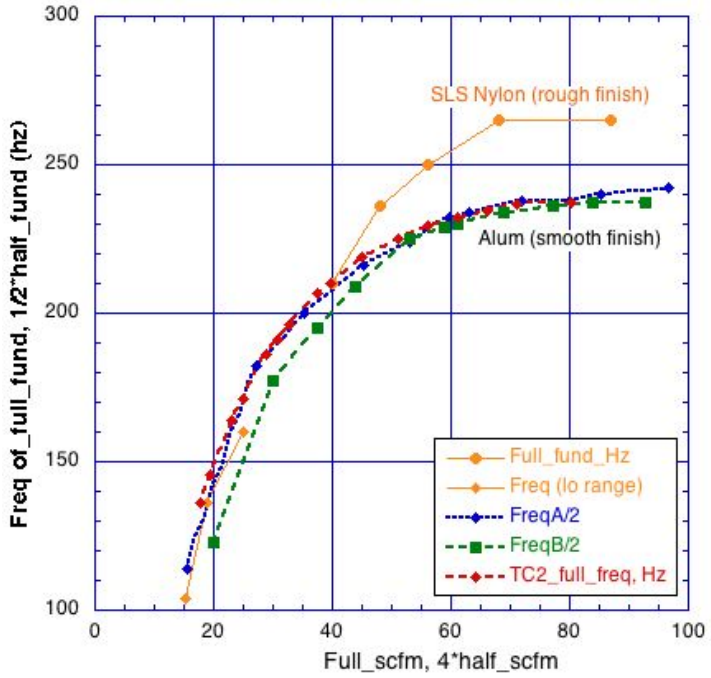


Fig. 6. Fundamental sweep frequency vs flow rate for full- and half-scale actuators, scaled to full-scale.
Orange: full-scale actuator, SLS nylon rough surface
Red: full-scaled actuator, aluminum machine surface
Blue: upper half-scale actuator, aluminum machine surface
Green: lower half-scale actuator, aluminum machine surface

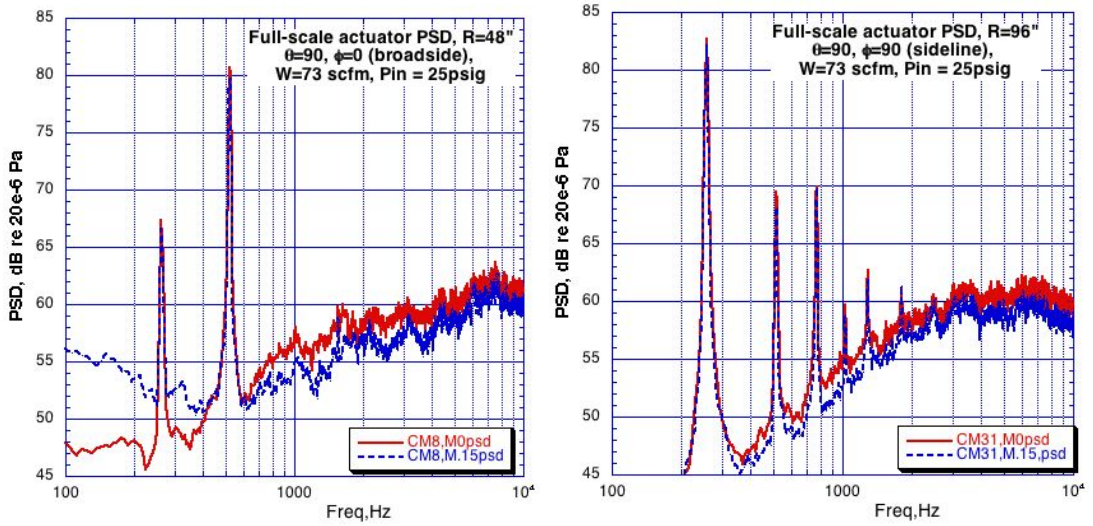


7a. 7b.

Fig. 7. Narrow band PSD of full-scale actuator, $P_{IN}$ = 25 psig, R = 48 in. Ambient flow M = 0 (red) and M = 0.15 (blue).
7a: broadside (θ =90˚, ϕ = 0˚)
7b: sideline (θ = 90˚, ϕ = 90˚)

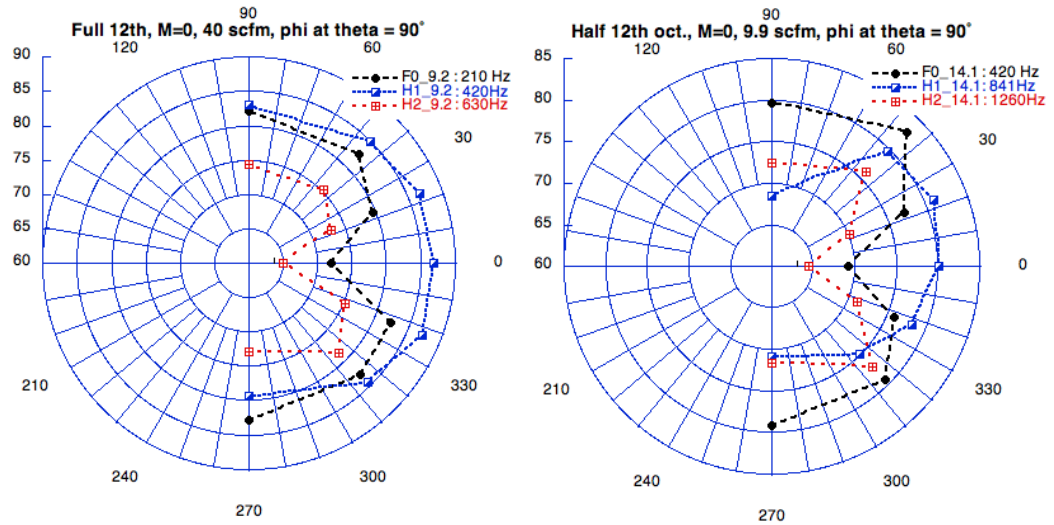


Fig. 8. Tone directivities: fundamental (black), 1st (blue) and 2nd (red) harmonics.
M = 0, W = 9.9 SCFM, R = 48 in, θ = 90˚. Full- (left) and half-scale (right) single actuators.

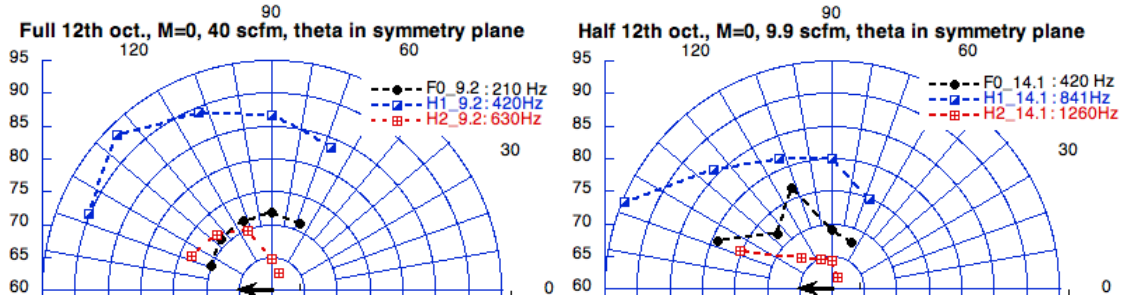


Fig. 9. Tone directivities: fundamental (black), 1st (blue) and 2nd (red) harmonics. M = 0, W = 9.9 SCFM, R = 48 in, ϕ = 0˚. Full- (left) and half-scale (right) single actuators. Flow is right to left.

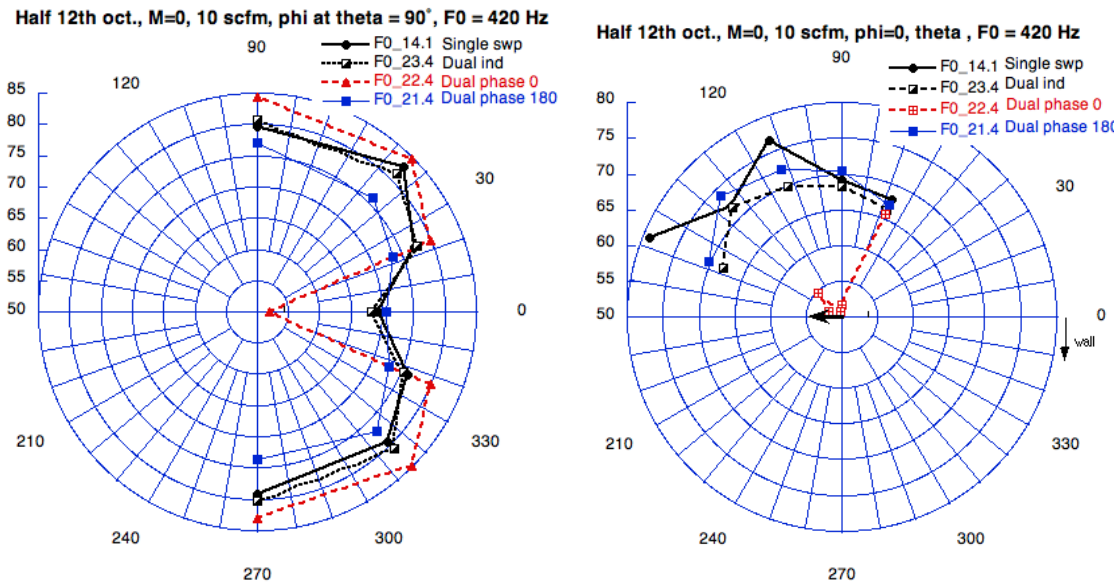


Fig. 10. Fundamental tone directivities of single- and dual-half scale actuators with phase control: Black: single (solid) and dual independent (dashed), red: dual in-phase, blue: dual out-of phase. M = 0, R = 48 in, W = 10 SCFM, $\theta = 90^{\circ}$ (left), $\phi = 0$ (right)

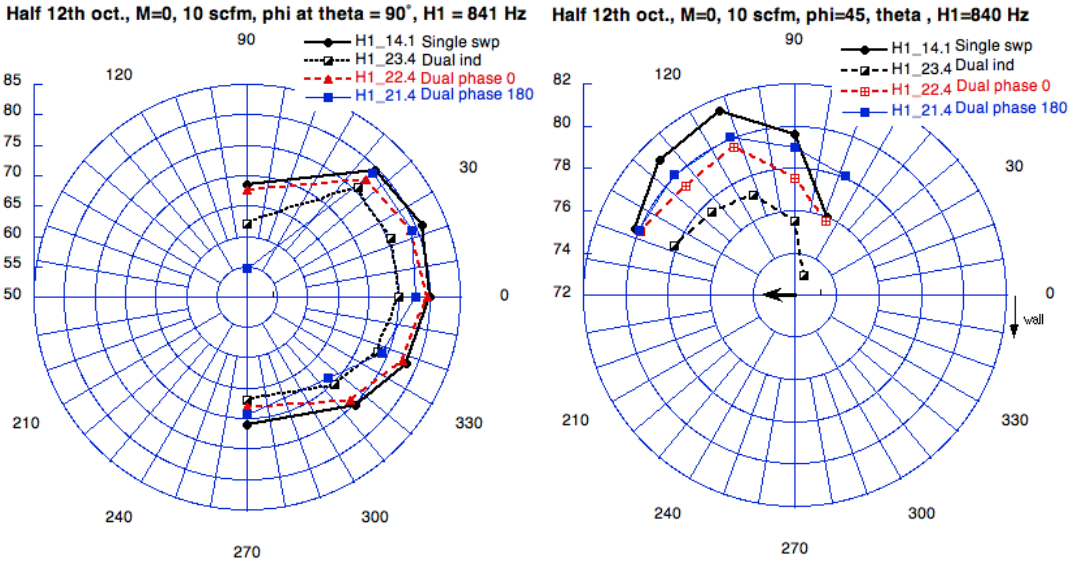


Fig. 11. 1st harmonic tone directivities of single- and dual-half scale actuators with phase control: Black: single (solid) and dual independent (dashed), red: dual in-phase, blue: dual out-of phase, M = 0, W = 10 SCFM, R = 48 in, $\theta = 90^{\circ}$ (left), $\phi = 0$ (right)

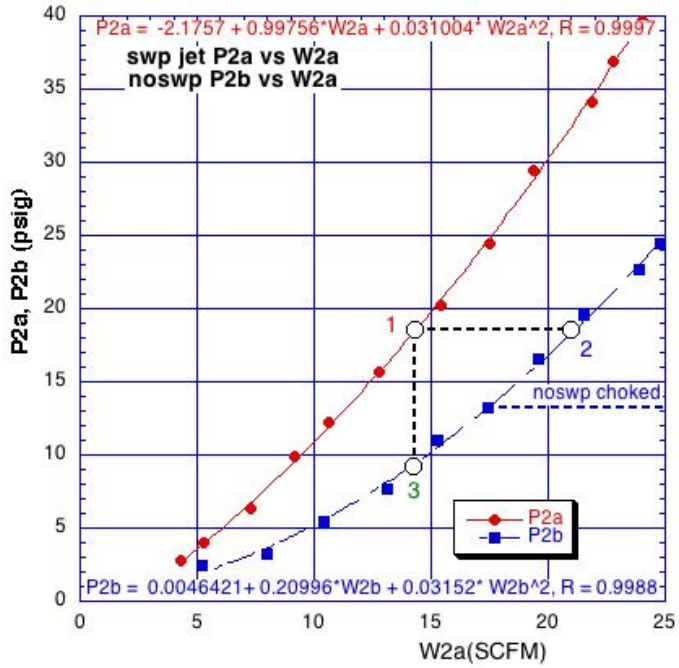


Fig. 12. Pressure drop vs flow rate for sweeping-jet (red) and non-sweeping jet (blue) actuators. The dashed lines connect flow conditions (1,2, 3) for the comparative plot in Fig. 13.

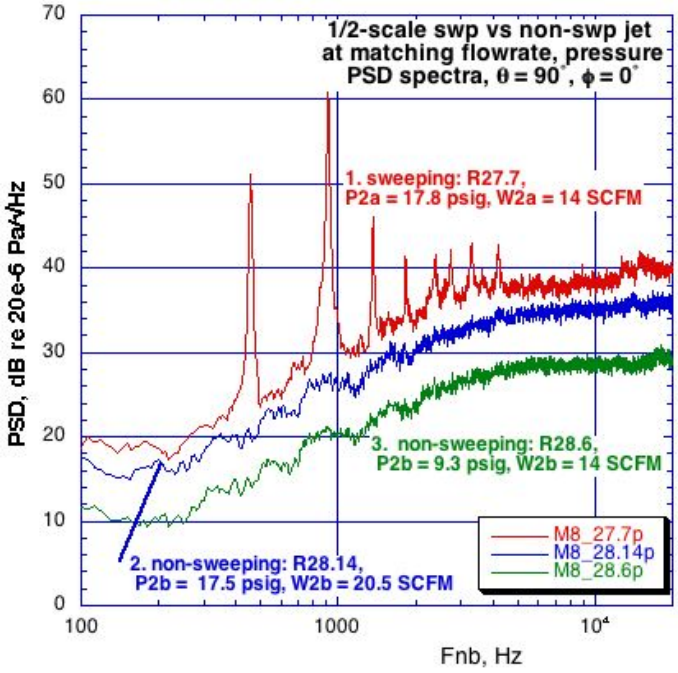


Fig. 13. Comparison half-scale narrow band spectra at 48 in, θ = 90˚, ϕ = 0˚ for:
Red- sweeping jet, Pin = 17.8 psig, W = 14 SCFM
Blue – non-sweeping jet, Pin = 17.5 psig, W = 20.5 SCFM
Green- non sweeping jet, Pin = 9.3 psig, W = 14 SCFM.

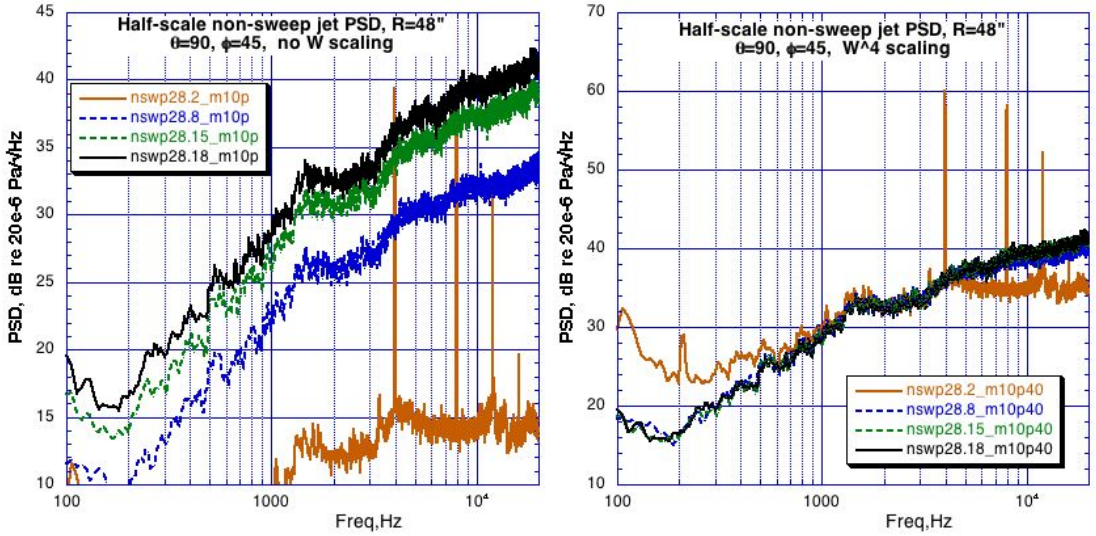


Fig. 14. Half-scale non-sweeping jet PSDs, R = 48 in, θ = 90˚, ϕ = 45˚, M = 0, unscaled (left) and scaled (right) with 4th power of flow rate, 7.1< W < 23.4 SCFM.

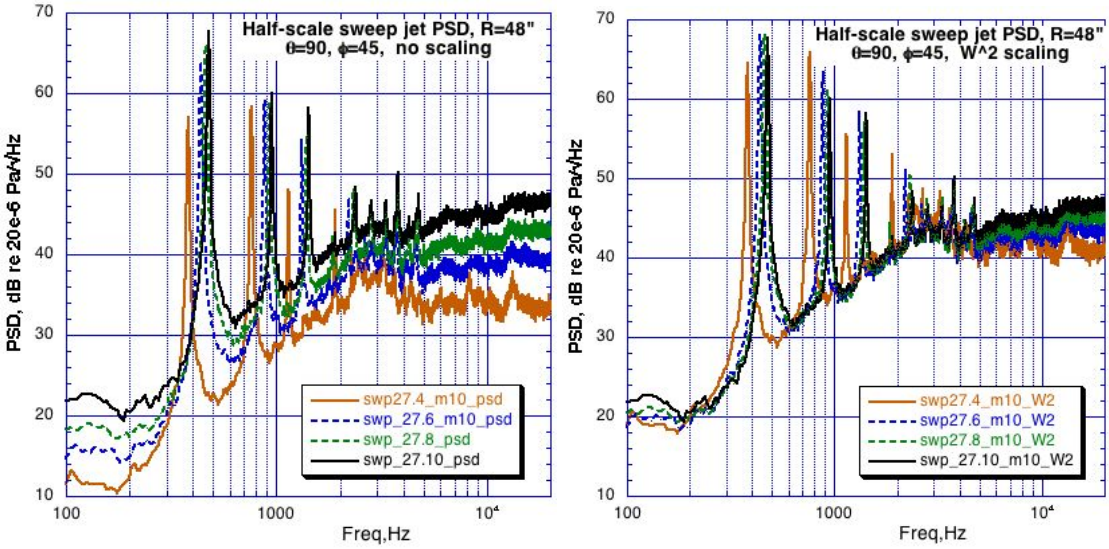


Fig. 15. Half-scale sweeping jet PSDs, R = 48 in, θ = 90˚, ϕ = 45˚, M = 0, unscaled (left) and scaled (right) with 2nd power of flow rate, 8.2 < W < 19.4 SCFM.

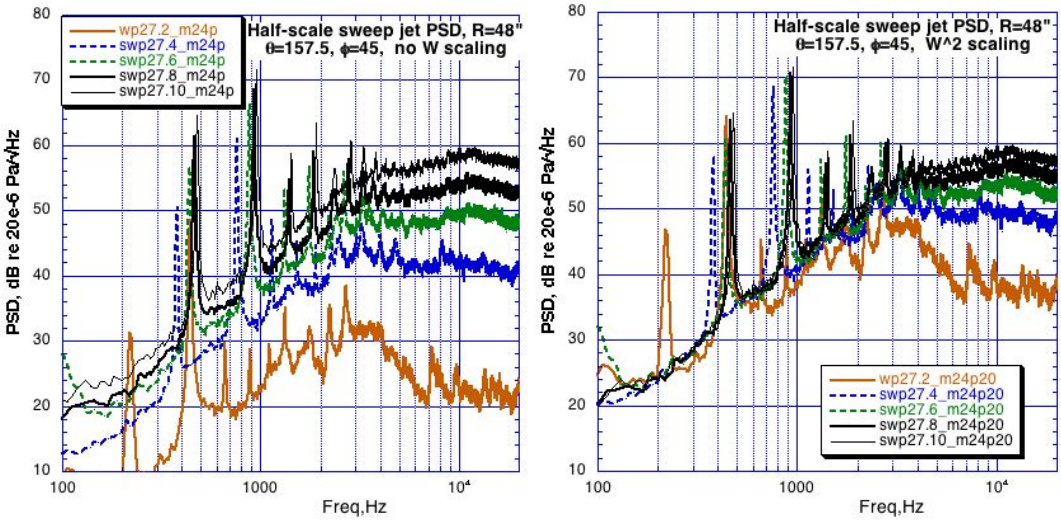


Fig. 16. Half-scale sweeping jet PSDs, R = 48 in, θ = 157.5˚, ϕ = 45˚, M = 0, unscaled (left) and scaled (right) with 2nd power of flow rate, 8.2 < W < 19.4 SCFM.